Journal of Organometallic Chemistry 880 (2019) 349–354

Contents lists available at ScienceDirect

Journal of Organometallic Chemistry

journal homepage: www.elsevier.com/locate/jorganchem

Ferrocenyl-functionalized carbon nanotubes with greatly improved surface reactivity for enhancing electrocapacitance

Yongfu Qiu [a], Xiaoting Wang [a], Huizhen Huang [c], Zhiyu Cheng [a, *], Xueyi Chang [a], Lin Guo [b, **]

[a] School of Environment and Civil Engineering, Guangdong Engineering and Technology Research Center for Advanced Nanomaterials, Dongguan University of Technology, Guangdong, 523808, People's Republic of China
[b] School of Chemistry and Environment, Beihang University, Beijing, 100191, People's Republic of China
[c] Department of Food Engineering, Zhangzhou Institute of Technology, Zhangzhou, 363000, People's Republic of China

ARTICLE INFO

Article history:
Received 16 October 2018
Received in revised form
7 November 2018
Accepted 9 November 2018
Available online 10 November 2018

Keywords:
Ferrocenyl-functionalized carbon nanotubes
Electrochemical double-layer capacitance
Supercapacitor

ABSTRACT

A series of ferrocenyl functionalized carbon nanotubes (CNT-Fc-n,n = 1,2,3) were synthesized and used as electrode materials for high performance supercapacitors. The results of galvanostatic charge-discharge measurement show that the specific capacitances of CNT-Fc-3 based electrode increase with the decrease of current densities. When the current density is 0.4 A g^{-1}, the maximum capacitance is 53.6 F g^{-1}. Ragone diagram, which shows that the symmetrical supercapacitor device based on CNT-Fc-3 electrode has typical symmetric capacitance characteristics. The energy density of CNT-Fc-3 based electrode under 0.1 kW kg^{-1} is calculated to be 5.0 Wh kg^{-1}, and 3.0 Wh kg^{-1} is kept in 0.5 kW kg^{-1}. In addition, the galvanostatic charge-discharge technique is used to test the stability of the cycle. The results show that the capacitance retention rate reaches 96.0% in 5000 cycles. In conclusion, ferrocenyl functionalized carbon nanotubes are ideal electrode materials for low cost and high efficiency electrochemical supercapacitors.

1. Introduction

As a new type of electrochemical energy storage device, supercapacitor (SC) has received extensive attention in recent years for its advantages of high power density, long cycle life, safe operation and environmental friendliness [1–5]. According to its working mechanism, electrochemical double-layer capacitance (EDLC) and pseudo-capacitor are two typical types. EDLC has better cycle stability, but its energy density is lower than that of pseudo-capacitor.

In recent years, the main strategies to improve the electrical density of carbon materials are: 1) adjusting and controlling the pore size and structure of carbon materials, making electrolyte ions penetrate, reducing the charge separation distance of electrochemical double layer [6–8]; 2) enlarging the specific surface area, the activity of electrochemical double layer was improved [6–8]; 3) doping agent such as metal and nonmetallic doping was introduced [9,10]; (4) pseudo-capacitive species were introduced on carbon electrode materials such as surface functional groups, transition metal oxides and conductive polymer [11–15].

In this paper, the synthesis of ferrocene-based functionalized carbon nanotubes and its application as electrode materials for high performance supercapacitors are reported. The electrochemical properties of ferrocenyl functionalized carbon nanotubes in 1.0 M Na_2SO_4 electrolyte were measured by three-electrode system. When the current density is 0.4 A g^{-1}, the maximum specific capacitance of the sample is 53.6 F g^{-1}, and the capacitance retention rate is 96.0% in 5000 cycles with 1.0 A g^{-1} current density.

2. Experimental section

2.1. Materials

Ferrocene (Macklin, purity 99%) and Multi-walled carbon nanotubes (MWCNTs, Chengdu Organic Chemicals Co. Ltd.) were used without further treatment as received. Other reagents were all commercial chemicals of analysis grade and purified following the

* Corresponding author.
** Corresponding author.
E-mail addresses: chengzy@dgut.edu.cn (Z. Cheng), guolin@buaa.edu.cn (L. Guo).

https://doi.org/10.1016/j.jorganchem.2018.11.014
0022-328X/

standard procedures. Water used in all experiments was deionized and filtrated by a Millipore purification apparatus with resistivity more than 18.0 MΩ cm.

2.2. Preparation of ferrocenyl-functionalized multi-walled carbon nanotubes

The synthetic routes for the ferrocenyl-functionalized multi-walled carbon nanotubes (denote as CNT-Fc) are shown in Fig. 1. In order to introduce ferrocenyl groups on the surface of the carbon nanotubes, MWCNTs were firstly treated to obtain carboxy-modified multi-walled carbon nanotubes (denoted as CNT-COOH) following the method reported by Burghard et al. with slightly improvement [16].

The typical steps for synthesis of CNT-COOH are as follows: MWCNTs (5 g) were added to nitric acid (300 mL, 69 wt %) and sonicated to ensure they were dispersed. The resulting suspension of MWCNTs was refluxed under magnetic stirring for 4 h at 130 °C to oxidize MWCNTs. The oxidized suspension of MWCNTs was cooled and filtered using sintered discs (G4, 3–4 μm pore diameter) and washed with deionized water. The oxidized MWCNTs retained on the sintered discs were dispersed in deionized water (280 mL) by sonication. An acidic solution of potassium permanganate (3.5 g) and perchloric acid (200 mL, 70 wt %) was then added to the stirring solution. The potassium permanganate was quenched after 10–30 min by the addition of a solution of citric acid (21.0 g). The suspension was filtered using sintered discs (G4, 3–4 μm pore diameter) and washed repeatedly to neutral with deionized water and alcohol. The resulting carboxy-modified MWCNTs (CNT-COOH, 4.9 g) were obtained by drying under vacuum at 40 °C for 12 h. The CNT-COOH were synthesized with difference periods of stirring time (4, 6 and 8 h) were denoted as CNT-COOH-n (***n*** = **1, 2, 3**).

The typical steps for synthesis of CNT-Fc are as follows: CNT-COOH-1 (1.5 g) was dispersed in dry dichlormethane (40 mL) by sonication, and then the suspension was cooled to 0 °C with stirring under an argon atmosphere. 1.0 mL of oxalyl chloride was added to the above suspension. The mixture was stirred at 0 °C for 1 h, and rised to room temperature for another 5 h. The resultant suspension was concentrated in vacuum at room temperature to obtain acyl chloride product (CNT-COCl). The acyl chloride product (CNT-COCl) was dispersed in 30 mL of dichlormethane again and added dropwise into a mixture of ferrocene (3.2 g, 16.9 mmol) and anhydrous aluminum chloride (2.3 g, 16.9 mmol) in 40 mL of dichlormethane for about 1 h under argon. After stirring 8 h, 30 ml of 5 mol L^{-1} hydrochloric acid solution was added slowly in the suspension to terminate the reaction. The suspension was filtered using sintered discs (G4, 3–4 μm pore diameter) and washed repeatedly to neutral with deionized water and alcohol. The resulting ferrocenyl-functionalized multi-walled carbon nanotubes (CNT-Fc-1, 1.7 g) were obtained by drying under vacuum at 40 °C for 12 h. CNT-Fc-2 or -3 was synthesized similarly, the only difference was raw materials using CNT-COOH-2 or -3, respectively.

2.3. Fabrication of CNT-Fc-n/Ni electrode and its device

The working electrode was prepared as follows: the mixing of CNT-Fc-*n* (80 wt %), acetylene black (10 wt %), and PTFE glue (10 wt %) using ethanol/water as the solvent was prepared and then the slurry was coated onto the nickel foam (1.0 cm × 1.0 cm) at 20.0 MPa and dried at 100 °C for 6 h. The active material mass of the electrode was about 5.0 mg. The devices of analog supercapacitor were assembled with filter paper/1.0 M Na_2SO_4 serving as separator and electrolyte between the working electrode and nano-carbon tube/nickel foam electrode.

2.4. Characterization

The morphologies of CNT-Fc-*n* ($n = 1, 2, 3$) and raw materials CNTs were characterized by scanning electron microscopy (SEM) using JEOL 6701F at an accelerating voltage of 5 kV. The XRD analyses were performed on a Rigaku Ultima IV X-ray diffractometer under Cu K_a radiation (wavelength $\lambda = 0.154$ nm) at a scanning speed of 0.025° s^{-1} over the 2θ range of 10–80° at room temperature. The X-ray photoelectron spectra (XPS) were obtained using a Kratos Axis Ultra Dldxps instrument equipped with a monochromatic Al K_a X-ray source. Fourier transform infrared spectroscopy (ATR-FTIR) was measured on a Thermo Nicolet 6700 spectrometer. The contact angles of samples were obtained from a surface tension meter (Dataphysics OCA20, Germany) at 25 °C. X-ray fluorescence (XRF) was obtained using a JEOL JSX-3400RII instrument.

Electrochemical measurements, such as, Cyclic voltammetry (CV), galvanostatic charge/discharge measurements, and electrochemical impedance spectroscopy (EIS) were carried out in a three-electrode system using a Gamry Reference 3000 electrochemical work station, 1.0 M Na_2SO_4 as aqueous electrolyte, CNT-Fc-*n*/Ni or CNT/Ni electrode as working electrode, Ag/AgCl (3.0 M KCl) and a Pt wire as the reference and counter electrodes, respectively.

3. Results and discussion

3.1. Structural characterization

The morphologies of CNT-Fc and raw materials CNTs were characterized by scanning electron microscopy (SEM), as shown in Fig. 2. The results showed that the diameters and morphologies of CNT-Fc have no obvious change compared with MWCNTs, indicating that the ferrocene content on the surface of CNTs was small and uniform. Fig. 3 shows a typical XRD patterns for CNT-Fc and CNT. Clearly seen that all the diffraction peaks of CNT-Fc and CNT can be indexed as a = b = 0.2464 nm and c = 0.6736 nm (PDF

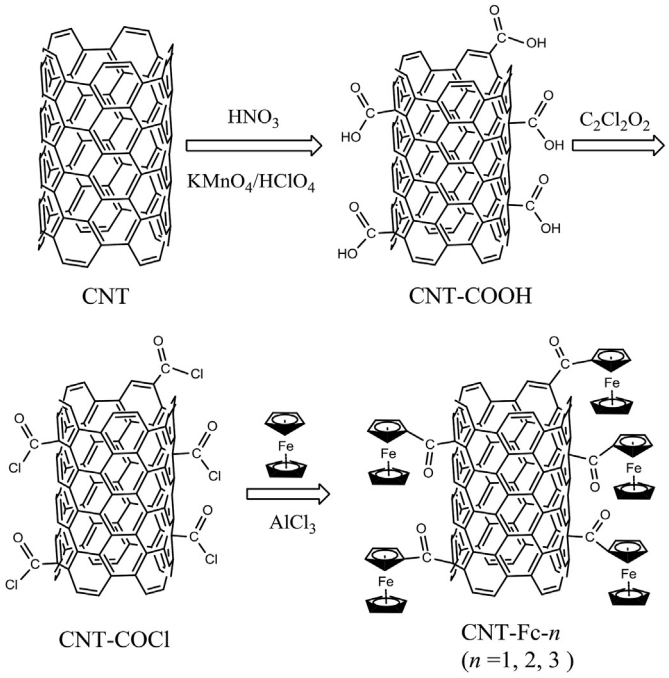

Fig. 1. Synthetic route for the ferrocenyl-functionalized carbon nanotubes CNT-Fc-*n* ($n = 1, 2, 3$).

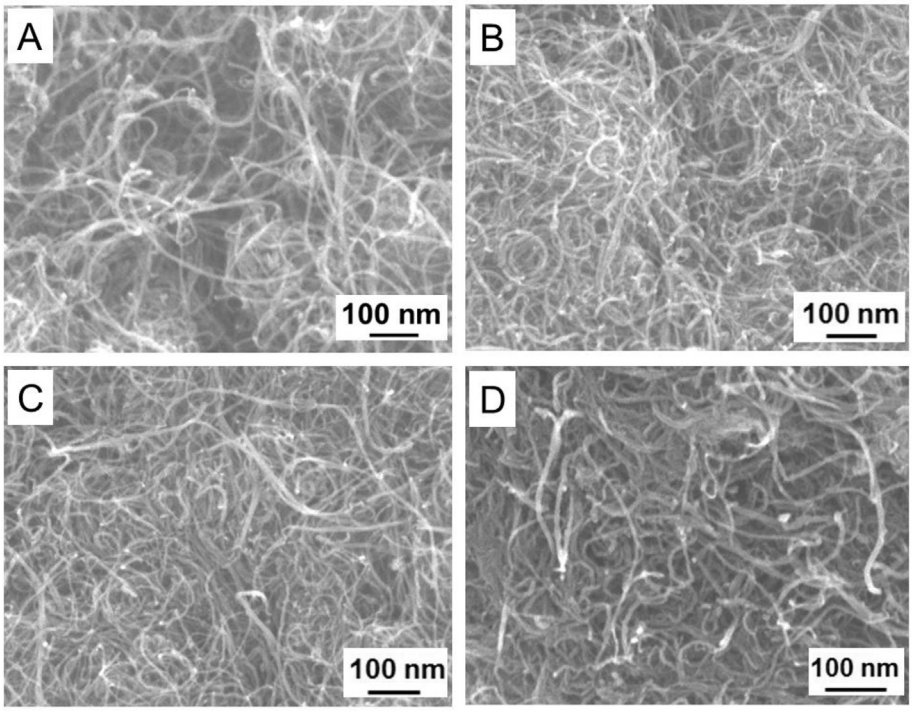

Fig. 2. The typical SEM images of (A) MWCNTs; (B) CNT-Fc-1; (C) CNT-Fc-2; (D) CNT-Fc-3.

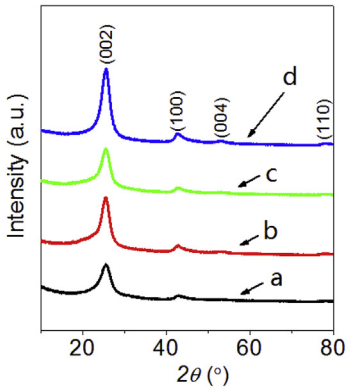

Fig. 3. The typical X-ray diffraction patterns of (a) MWCNTs; (b) CNT-Fc-1; (c) CNT-Fc-2; (d) CNT-Fc-3.

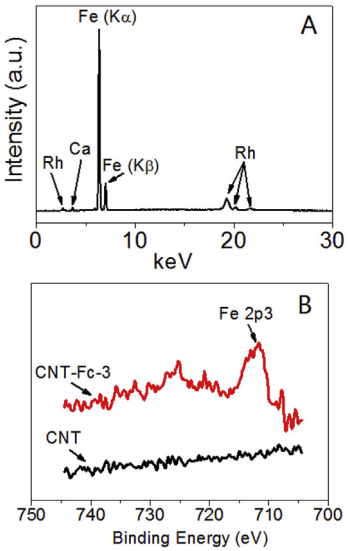

Fig. 4. **(A)** The XRF patterns of as-prepared CNT-Fc; (B) XPS spectrum for the CNTs and as-prepared CNT-Fc.

#08–0415), suggesting that the crystal structure of CNT-Fc remains unchanged, and a small amount of ferrocene on the surface of CNTs cannot produce diffraction peaks and be detected.

In Fig. 4A, the elements of CNT-Fc were analyzed by using x-ray fluorescence (XRF). The results showed that except carbon, the other element is Iron. The low contents of Calcium and Rhodium elements with "Ghost Peaks" are from the instrument. X-ray fluorescence spectroscopy (XRF) cannot detect Carbon and Oxygen because their fluorescence yield is very low. The X-ray photoelectron spectra (XPS) in Fig. 4B further confirms the presence of a small amount of Iron on the CNT-Fc surface.

Attenuated Total Internal Reflectance Fourier Transforminfrared Spectroscopy (ATR-FTIR) was used to determined molecular scale information on the surfaces of samples MWCNTs and CNT-Fc-n. Before measurements, these samples were heated in vacuum at 60 °C for 12 h to remove the physical adsorbed water. In Fig. 5, the samples CNT-Fc-1, CNT-Fc-2, and CNT-Fc-3 have obvious peaks at 3095, 1650, 1454, 1105, 1001, and 829 cm^{-1}, but no corresponding peaks could be found in MWCNTs, which means that the groups of C=O and single substituted ferrocenyl groups were generated after treatment. The coexistence of C=O and single substituted ferrocenyl groups suggests that the −CO-Fc groups were successfully introduced on the surface of MWCNTs.

In order to characterize the wettability of surface, the water contact angle measurement of CNT-Fc-*n* ($n = 1, 2, 3$) and raw materials CNTs was carried out. The contact angle is the angle measured through the liquid, where a liquid–vapor interface meets a solid surface, which quantifies the wettability of a solid surface by

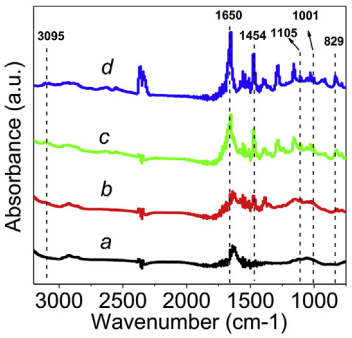

Fig. 5. ATR-FTIR spectra recorded for (a) MWCNTs; (b) CNT-Fc-1; (c) CNT-Fc-2; (d) CNT-Fc-3.

a liquid via the Young equation: $Y_{SG} - Y_{SL} - Y_{LG}\cos\theta_C = 0$, where Y_{SG}, Y_{SL} and Y_{LG} are the solid– vapor interfacial energy, the solid–liquid interfacial energy and the liquid–vapor interfacial energy, and θ_C is the equilibrium contact angle. In Fig. 6, the descending contact angles of CNT, CNT-Fc-1, CNT-Fc-2, and CNT-Fc-3 could be observed. The enhancement of surface hydrophilicity is ascribed to the uptake of ferrocenyl groups on MWCNTs after grafting. These ferrocenyl groups are considered to be the strong polar centers of absorbed water molecules.

3.2. Electrochemical properties

In Fig. 7A, the Cyclic voltammograms (CV) of MWCNT, CNT-Fc-1, CNT-Fc-2, and CNT-Fc-3 could be observed. The enclosed area of CV increases in the order of MWCNT, CNT-Fc-1, CNT-Fc-2, and CNT-Fc-3, which indicates that the connected ferrocenyl groups has a greatly effect on the redox properties of samples. Compared with the quasi-rectangular of CV of MWCNT, it is interesting that a small peak at ca. 0–0.3 V can be observed in the CV curves for CNT-Fc-*n* ($n = 1, 2, 3$), which may be due to the electron delocalization of ferrocenyl groups in the redox process.

Fig. 7B shows the galvanostatic charge-discharge curves of the MWCNT, CNT-Fc-1, CNT-Fc-2, and CNT-Fc-3 based electrodes at current densities 0.4 A g^{-1}. These curves generally show symmetrical and linear profiles, indicating that the samples have good supercapacitive behaviors. The charging and discharging time increasing in the order of MWCNT, CNT-Fc-1, CNT-Fc-2, and CNT-Fc-3 further confirm that the connected ferrocenyl groups have effect on the redox properties of samples.

Fig. 7C shows the CV curves of CNT-Fc-3 at different scanning rates. The CV curves exhibit quasi-rectangular shape at low scanning rate (10 mV s^{-1}), and show a little deviation and enlarged

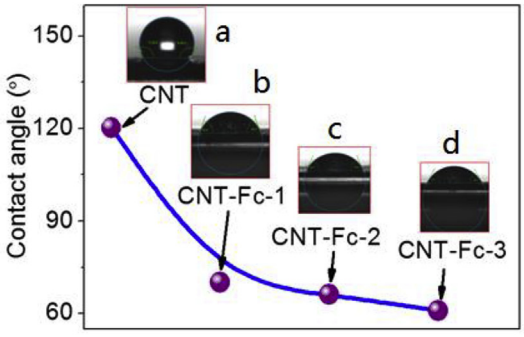

Fig. 6. Contact angle of samples as function of ferrocenyl-groups grafting degree: (a) MWCNTs; (b) CNT-Fc-1; (c) CNT-Fc-2; (d) CNT-Fc-3.

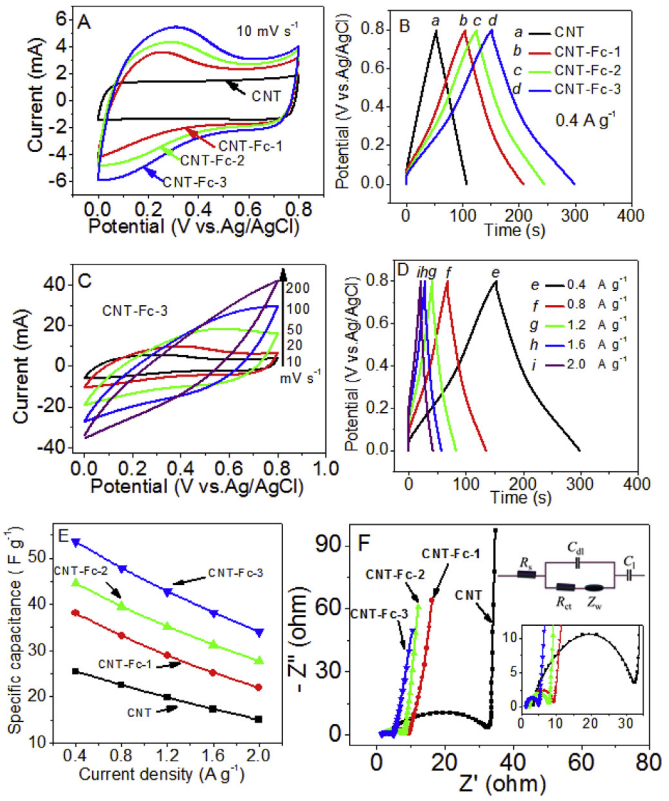

Fig. 7. (A) Cyclic voltammograms (CV) collected at scan rate 10 mV s^{-1} for MWCNTs, CNT-Fc-1, CNT-Fc-2 and CNT-Fc-3; (B) Charge-discharge curves at 0.4 A g^{-1} for MWCNTs, CNT-Fc-1, CNT-Fc-2 and CNT-Fc-3; (C) CV collected at different scan rates for CNT-Fc-3; (D) Charge-discharge curves at various current densities for CNT-Fc-3; (E) Specific capacitance calculated based on charge-discharge curves as a function of current density. (F) Nyquist electrochemical impedance spectra of MWCNTs, CNT-Fc-1, CNT-Fc-2 and CNT-Fc-3 based electrode; the insets are the corresponding enlarged curve and well-fitted equivalent circuit.

enclosed-area at high scanning rates (>10 mV s^{-1}). This suggests that the CV processes were controlled by redox reaction of the connected ferrocenyl group.

Fig. 7D shows the galvanostatic charge-discharge curves of the CNT-Fc-3 based electrodes at different current densities. These curves generally are symmetricay and linear profiles, indicating that CNT-Fc-3 has good supercapacitive behavior. The specific capacitances calculated from charge-discharge curves as a function of current density are shown in Fig. 7E [17]. The specific capacitances decrease with increasing current densities for all samples. When the current density is 0.4 A g^{-1}, the maximum capacitance of CNT-Fc-3 is 53.6 F g^{-1}. For the raw materials MWCNTs, of the same current density, the value is 2.1 times higher than that of 25.5 F g^{-1}, which indicates that the connected ferrocenyl groups can greatly improve surface reaction activity and increase the capacitance [8].

Fig. 7F shows the Nyquist plots of CNT-Fc-*n* ($n = 1, 2, 3$)-based electrode in 1.0 M Na_2SO_4 aqueous electrolyte with a frequency range of 10^{-2} to 10^5 Hz. Insets are the equivalent circuit diagram and the enlarged high-frequency range plots. The small semicircle with upward deviation in the high-frequency region reflects the low charge-transfer resistance (R_{ct}) and rough surface of CNT-Fc-*n* ($n = 1, 2, 3$)-based electrodes. The charge transfer resistances (R_{ct}) of MWCNT, CNT-Fc-1, CNT-Fc-2, and CNT-Fc-3-based electrodes based on the diameters of semicircle are 17.3, 5.1, 4.4 and 3.1 Ω. The straight line with about 70° upward in the low- and mid-frequency region can be observed, which suggests that CNT-Fc-*n* (n = 1, 2, 3)-based electrode has typical supercapacitor performance.

In Fig. 8A, the CV curves are collected at different scanning rates for the fabricated symmetrical supercapacitor devices based on CNT-Fc-3 electrode. The CV curves exhibit quasi-rectangular shapes and their enclosed-areas become larger with higher scanning rates, which indicate that they have typical symmetric capacitance characteristics. In Fig. 8B, the charge-discharge curves at various current densities are symmetrical and linear profiles, which further confirm its good supercapacitive properties. Fig. 8C shows the Ragone plot (energy density vs. power density) of the two fabricated symmetrical supercapacitor based on CNT-Fc-3 and CNT electrodes, respectively. The calculated results show that when the power density is 0.1 kW kg^{-1}, the energy density of CNT-Fc-3-based electrodes is 5.0 Wh kg^{-1}, while the power density is 0.5 kW kg^{-1}, the energy density 3.0 Wh kg^{-1} is kept. We can see that the calculated energy densities at various power densities for CNT-Fc-3-based electrodes are higher than those of MWCNT-based symmetrical supercapacitor. This indicates that CNT-Fc-3-based symmetrical supercapacitor has good rate characteristics. In addition, the capacitance retention measured by the galvanostatic charge/discharge technique at a constant current density of 1.0 A g^{-1} over 5000 cycles is shown in Fig. 8D. After 5000 cycles, the specific capacitance is reduced to about 96.0% of the initial capacitance. This indicates that CNT-Fc-3-based electrodes reveal good stability over long charge/discharge processes. Fig. 8E is the Light-emitting diode (LED) lighting demonstration with the diode driven by a symmetrical supercapacitor that is composited by the CNT-Fc-3-based electrodes. The diode driven by the supercapacitors could be lighting about 23 s after 10 s charged by a 2 V DC power supply, which shows their good supercapacitive properties.

4. Conclusions

In summary, a series of ferrocene-based functionalized carbon nanotubes (CNT-Fc-*n*, $n = 1, 2, 3$) were synthesized and their applications in high performance supercapacitor electrode materials were reported. The morphologies, crystal structures, the elements analysis and the surface wetting of CNT-Fc-n were characterized by SEM, XRD, XRF, XPS and water contact angle measurement. ATR-FTIR analysis showed that -CO-Fc group was successfully introduced on the surface of MWCNTs. The results of galvanostatic charge-discharge measurement show that the maximum capacitance of CNT-Fc-3 based electrode is 53.6 F g^{-1} when the current density is 0.4 A g^{-1}. At the same current density, this value is 2.1 times higher than the 25.5 Fg^{-1} of raw MWCNTs. The charge transfer resistances (R_{ct}) of MWCNT, CNT-Fc-1, CNT-Fc-2, and CNT-Fc-3 based on semicircle diameters are 17.3, 5.1, 4.4 and 3.1 Ω.

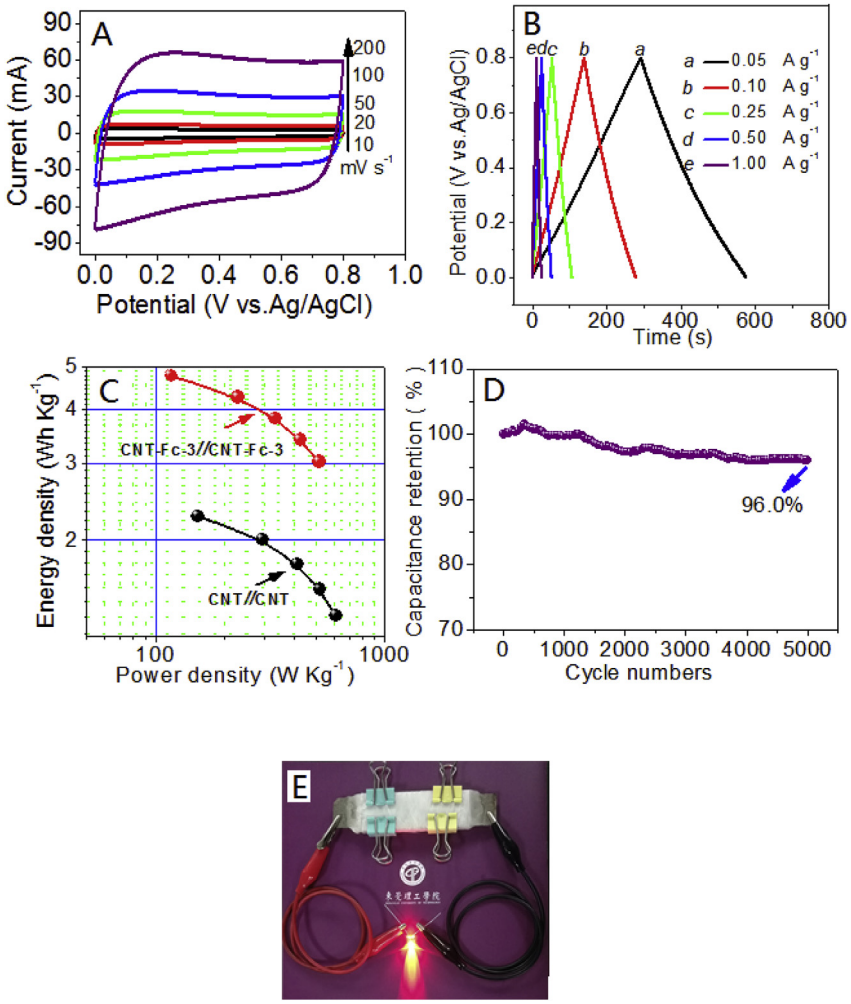

Fig. 8. (A) The CV curves are collected at different scan rates for the fabricated symmetrical supercapacitor based on CNT-Fc-3 electrodes; (B) Charge-discharge curves at various current densities for the fabricated symmetrical supercapacitor based on CNT-Fc-3; (C) The Ragone plots for the two fabricated symmetrical supercapacitor based on CNT-Fc-3 and MWCNTs electrode, respectively. (D) Capacitance retention test over 5000 cycles at a current density of 1.0 A g^{-1} for the fabricated symmetrical supercapacitor based on CNT-Fc-3; (E) Light-emitting diode (LED) lighting demonstration with the diode driven by a symmetrical supercapacitor composited by CNT-Fc-3-based electrodes.

The Ragone plot shows that the fabricated symmetrical supercapacitor devices based on CNT-Fc-3 electrode have typical symmetric capacitance characteristics. The energy density of CNT-Fc-3-based electrodes under 0.1 kW kg^{-1} is calculated to be 5.0 Wh kg^{-1} and 3.0 Wh kg^{-1} is kept in 0.5 kW kg^{-1}. Moreover, cyclic stability was measured by galvanostatic charge-discharge technique at constant current density of 1.0 A g^{-1} in 1.0 M Na_2SO_4 aqueous electrolyte. The results show that the capacitance retention rate of ferrocene-based functionalized carbon nanotubes can reach 96.0% during 5000 cycles. Therefore, ferrocene-based functionalized carbon nanotubes are ideal electrode materials for low-cost and high-efficiency electrochemical supercapacitors.

Acknowledgements

The work described in this paper was supported by the Technology Planning Project of Guangdong Province (No. 2016B090918006 and 2015B090927007), the Guangdong Innovation Team Project for Colleges and Universities (No. 2016KCXTD023), We thank Qiu Yan (1941308558@qq.com) for her linguistic assistance during the preparation of this manuscript.

References

[1] P. Huang, C. Lethien, S. Pinaud, K. Brousse, R. Laloo, V. Turq, M. Respaud, A. Demortiere, B. Daffos, P.L. Tabema, B. Chaudret, Y. Gogotsi, P. Simon, On-chip and freestanding elastic carbon films for micro-supercapacitors, Science 351 (2016) 691–695.
[2] C.L. Tan, X.H. Cao, X.J. Wu, Q.Y. He, J. Yang, X. Zhang, J.Z. Chen, W. Zhao, S.K. Han, G.H. Nam, M. Sindoro, H. Zhang, Recent advances in ultrathin two-dimensional nanomaterials, Chem. Rev. 117 (2017), 6225-6331.
[3] M. Salanne, B. Rotenberg, K. Naoi, K. Kaneko, P.L. Taberna, C.P. Grey, B. Dunn, P. Simon, Efficient storage mechanisms for building better supercapacitors, Nat. Energy 1 (2016) 16070.
[4] Y.G. Wang, Y.F. Song, Y.Y. Xia, Electrochemical capacitors: mechanism, materials, systems, characterization and applications, Chem. Soc. Rev. 45 (2016) 5925–5950.
[5] A. Gonzalez, E. Goikolea, J.A. Barrena, R. Mysyk, Review on supercapacitors: technologies and materials, Renew. Sustain. Energy Rev. 58 (2016) 1189–1206.
[6] Q. Wang, J. Yan, Z.J. Fan, Carbon materials for high volumetric performance supercapacitors: design, progress, challenges and opportunities, Energy Environ. Sci. 9 (2016) 729–762.
[7] X.L. Yan, X.J. Li, Z.F. Yan, S. Komarneni, Porous carbons prepared by direct carbonization of MOFs for supercapacitors, Appl. Surf. Sci. 308 (2014) 306–310.
[8] Z. Cheng, P. Liu, B. Guo, Y. Qiu, P. Xu, H. Fan, Surface activation of carbon paper with potassium dichromate lotion and application as a supercapacitor, Appl. Surf. Sci. 349 (2015) 833–838.
[9] B. Li, F. Dai, Q.F. Xiao, L. Yang, J.M. Shen, C.M. Zhang, M. Cai, Nitrogen-doped activated carbon for a high energy hybrid supercapacitor, Energy Environ. Sci. 9 (2016) 102–106.
[10] Y.J. Li, G.L. Wang, T. Wei, Z.J. Fan, P. Yan, Nitrogen and sulfur co-doped porous carbon nanosheets derived from willow catkin for supercapacitors, Nanomater. Energy 19 (2016) 165–175.
[11] L. Wang, Y.Z. Han, X. Feng, J.W. Zhou, P.F. Qi, B. Wang, Metal-organic frameworks for energy storage: batteries and supercapacitors, Coord. Chem. Rev. 307 (2016) 361–381.
[12] Y.X. Zeng, M.H. Yu, Y. Meng, P.P. Fang, X.H. Lu, Y.X. Tong, Iron-based supercapacitor electrodes: advances and challenges, Adv. Energy Mater. 6 (2016) 1601053.
[13] Y. F Qiu, H.B. Fan, X.Y. Chang, H.F. Dang, Q. Luo, Z.Y. Cheng, Novel ultrathin Bi_2O_3 nanowires for supercapacitor electrode materials with high performance, Appl. Surf. Sci. 434 (2018) 16–20.
[14] J. Xiang, K. Sato, H. Tokue, K. Oyaizu, C.L. Ho, H. Nishide, W.Y. Wong, M.D. Wei, Eur. J. Inorg. Chem. 7 (2016) 1030–1035.
[15] Z.G. Meng, K. Sato, T. Sukegawa, K. Oyaizu, C.L. Ho, J. Xiang, Y.H. Feng, Y.H. Lo, H. Nishide, W.Y. Wong, J. Organomet. Chem. 812 (2016) 51–55.
[16] M. Burghard, V. Krstic, G. Duesberg, G. Philipp, J. Muster, S. Roth, Carbon SWNTs as wires and structural templates between nanoelectrodes, Synth. Met. 103 (1999) 2540–2542.
[17] A. Burke, Ultracapacitors: why, how, and where is the technology, J. Power Sources 91 (2000) 37–50.